Nuclear Instruments and Methods in Physics Research A 760 (2014) 98–106

Contents lists available at ScienceDirect

Nuclear Instruments and Methods in Physics Research A

journal homepage: www.elsevier.com/locate/nima

Performance of resistive-charge position sensitive detectors for RBS/Channeling applications

P.A. Miranda [a,*], U. Wahl [a], N. Catarino [c], M. Ribeiro da Silva [b], E. Alves [c]

[a] Centro de Ciências e Tecnologias Nucleares, Instituto Superior Técnico, Universidade de Lisboa, 2696-953 Sacavém, Portugal
[b] Centro de Física Nuclear da Universidade de Lisboa, Avenida Prof. Gama Pinto 2, 1649-003 Lisboa, Portugal
[c] Instituto de Plasmas e Fusão Nuclear, Instituto Superior Técnico, Universidade de Lisboa, 2696-953 Sacavém, Portugal

ARTICLE INFO

Article history:
Received 17 March 2014
Received in revised form
5 May 2014
Accepted 18 May 2014
Available online 2 June 2014

Keywords:
Position sensitive detector
RBS/Channeling
Lattice location

ABSTRACT

The performance of two types of 1×1 cm^2 photodiode position sensitive detectors (PSDs) based on resistive charge division was evaluated for their use in Rutherford Backscattering/Channeling (RBS/C) experiments in blocking geometry. Their energy resolution was first determined for $\sim$5.5 MeV alpha particles from a radioactive sources, and values of full width half maximum (FWHM) of 22 keV and 33 keV were achieved using a shaping time constant of $\tau = 2.0$ μs. Additional tests were performed using backscattered ^{4}He particles from the 2.0 MeV beam of a Van de Graaff accelerator. While the 22 keV FWHM detector failed after exposure to less than 5×10^6 cm^{-2} ^{4}He particles, the other did not show any noticeable deterioration due to radiation damage for a fluence of 4×10^8 cm^{-2}. For this type of PSD position resolution ($\tau = 0.5$ μs) standard deviations of $\Delta L = 0.072$ mm at $\sim$5.5 MeV and $\Delta L = 0.247$ mm at 1.1 MeV were achieved.

RBS/Channeling experiments using PSD were performed on several crystalline samples, showing that this setup seems suitable for lattice location studies, particularly for heavy ions implantation ($D \gtrsim 10^{15}$ at/cm^2) on light substrates like Si, SiC, and AlN.

1. Introduction

Several methods of ion beam analysis, e.g. elastic recoil detection analysis (ERDA) [1] and Rutherford Backscattering/Channeling (RBS/C) in blocking geometry [2] or alpha emission channeling from radioactive isotopes [3,4] rely on the position-sensitive detection of light or heavy ions. Since such types of applications require the exposure of the position-sensitive detector (PSD) to relatively high particle fluences, the resulting radiation damage in the detector is a serious issue. In particular for Si-based PSDs it usually demands the replacement of the device at regular intervals, which may be as often as several times per year for very intensive uses. Besides energy and position resolution and achievable count rate, the radiation hardness and the price of the sensor are therefore considerable factors in judging the usefulness of typical Si PSD systems for charged particle detection.

PSDs using the principle of resistive charge division (RCD) have been introduced already in the early 1960s [5] and a very good review on the subject was given in 1979 by Lægsgaard [6]. A major advantage of the RCD principle is that such types of detectors can be mass-produced at relatively low cost and as a matter of fact RCD-PSDs are manufactured in large numbers as position-sensitive photodiodes for optical applications. Although not designed for this purpose, the use of such photodiode PSDs for applications in charged particle detection has been reported previously in the literature, e.g. [7,4,8–10]. Since they are nowadays available at prices as low as $\sim$100 EUR per cm^2 of detection area, photodiode RCD-PSDs may represent a very attractive option as Si-based PSDs for the above-mentioned applications. In the course of the EU-funded SPIRIT project we have assessed the usefulness of several different types of PSDs (both RCD and pixel detectors) for their use in RBS/C experiments in blocking geometry. While in this paper we address the characterization of two types of RCD-PSDs, subsequent publications [11] will report on the use of pixel detectors of the Timepix/Medipix type [12,13] for the same purpose.

RBS/C experiments are one of the standard methods of ion beam analysis for crystalline materials [2,14–17], e.g. for determination of amount and depth distribution of lattice disorder, the composition and thickness of amorphous surface layers, the lattice location of heavy impurity atoms in light matrices etc. The two most commonly used experimental arrangements for RBS/C are sketched in Fig. 1(a) and (b). In both cases the orientation of the crystal with respect to the beam is usually changed in the form of an angular scan in the course of which at a certain angle the channeling condition is fulfilled for the ingoing particles, whereas the backscattered particles usually follow trajectories along "random" crystal orientations. In case (a) backscattered particles are

* Corresponding author.
E-mail address: pjmirand@gmail.com (P.A. Miranda).

http://dx.doi.org/10.1016/j.nima.2014.05.062
0168-9002/

measured using a well-collimated Si surface barrier detector (SSB). This arrangement combines best energy and kinematic resolution and is hence usually applied for experimental tasks where good depth resolution is required, however, it suffers from a relatively small solid angle of detection. In case (b) the solid angle of detection is increased by using a large area annular Si detector, which the beam passes through a small hole. With this method less accurate depth profiling is possible since on the one hand large area annular detectors have worse energy resolution and on the other hand also the kinematic spread of backscattered particles is larger due to the larger opening angle. This method is often applied e.g. for lattice location studies of impurities, where lower limits of detection are critical but worse depth resolution can be tolerated. A third alternative is shown in Fig. 1(c) and is for instance described also in Ref. [2]: the beam particles enter the single crystal in random directions, whereas the sample is oriented so that a low-index crystallographic axis points towards a position-sensitive detector. In this case the backscattered particles undergo blocking effects by atomic rows and planes on their way out of the crystal. The feasibility of this approach is based on the rule of reversibility of particle trajectories, as is discussed in Ref. [2] and references therein. The solid angle of detection for this arrangement is in between cases (a) and (b). The advantage of this method is that samples are very easy to orient towards the detector and that the two-dimensional blocking patterns contain more information than simple one-dimensional angular scans. In addition, the normalization of the counting time per angular position to the integrated beam current is not necessary any more, and errors introduced by the finite precision and reproducibility of goniometers are reduced since no rotations of the emitting crystal are necessary during the measurement itself.

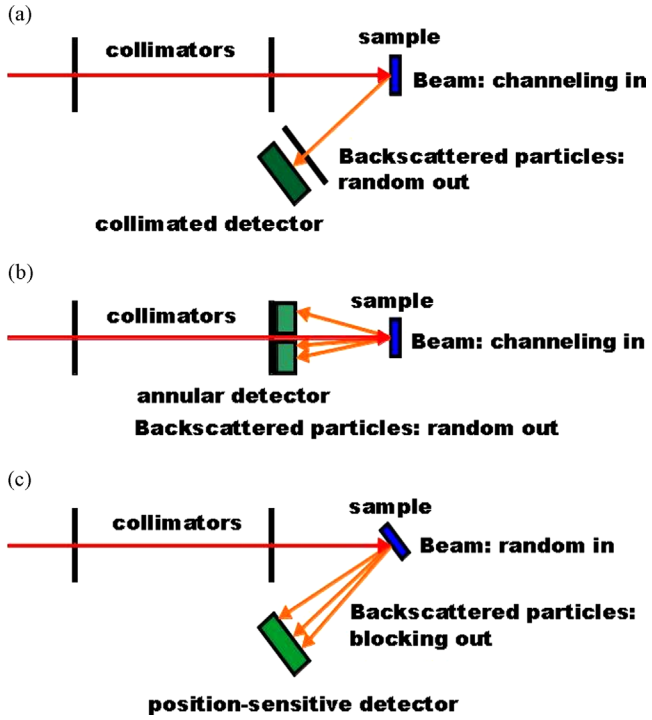

Fig. 1. Comparison of the principles of ion beam channeling. In (a) a collimated detector is used to perform conventional channeling experiments achieving better depth resolution while in (b) the use of an annular detector increased the efficiency of the spectroscopy system but the kinematic energy spread become significant. In (c) a two-dimensional position sensitive detector with intermediate solid angle allows not only an easier sample orientation but also to obtain 2D patterns for a reasonable collection time.

2. Experimental arrangements

While resistive charge division PSDs usually consist of rectangular Si diodes, several configurations can be realized for the arrangement of the resistive charge division layers and the readout electrodes. While some types use one single RCD layer with four readout electrodes of varying shape on the same side (so-called tetra-lateral type), cf. Refs. [18,19], photodiodes commonly have separate resistive layers on the front and back of the device, each connected to two readout electrodes (duo-lateral type). The detectors utilized in this study, which use the last approach, were two Position Sensing Photodiodes the first one a PSD Model DL100-7 CERpin from Silicon Sensor (company now named First Sensor) and a PSD Model 2L10UV_SU72 from SiTeK Electro Optics. These PSDs basically consist of a p-i-n-diode of square shape of 10×10 mm^2 with a sensitive depth of around 300 μm, made from a highly resistive single-crystalline Si wafer, on which 4 electrodes have been fixed on opposite sides such as indicated in Fig. 2.

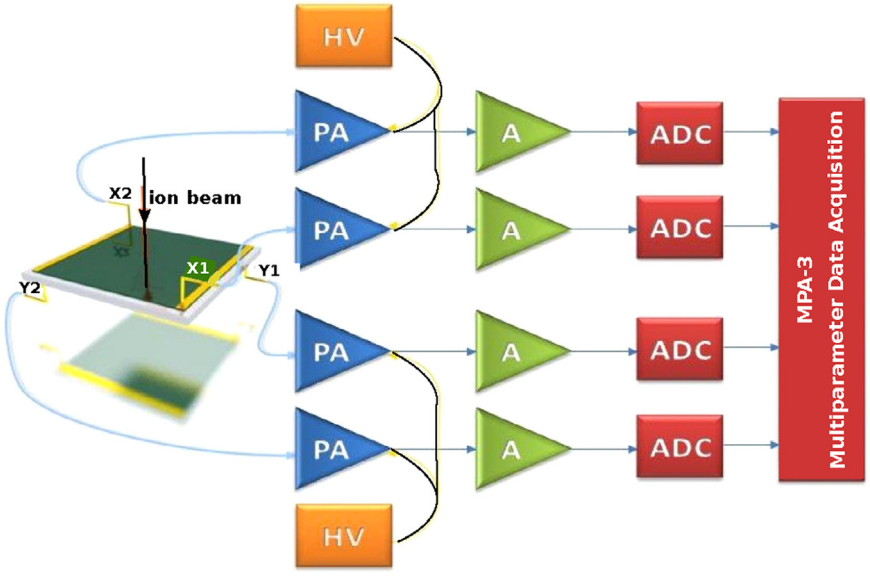

Fig. 2. Block diagram of the electronics used to determine the energy and position resolution of the PSD detector. The same setup was afterwards utilized in order to carry out lattice location studies during RBS/C experiments.

As specified by the manufacturers, the detector capacitance in both cases should be typically 75–100 pF at reverse voltages of 10–15 V, and inter-electrode resistances around 12 k Ω. When the resistances were measured for the first time in vacuum, they were found to fall into the range $11-17\ \mathrm{k}\Omega$, well within manufacturer specified tolerance. Both detectors contain a thin oxide layer of SiO_2 on the surface whose thickness was specified by the manufacturers to be less than 100 nm.

When a charged particle impinges on the detector at position (x,y) and loses the energy E by the creation of electron–hole pairs in the sensitive region, four different charges are collected in coincidence at the four electrodes of the device. The charge pulses are then picked up by Ortec 142B charge-sensitive preamplifiers and Canberra 2022 main shaping amplifiers and further processing is accomplished by passing the four amplified signals (E_1, E_2, E_3, E_4) directly to Silena 7423/UHS ADCs. Subsequently, the four digitized ADC signals are sent to a PC where a Fast ComTec GmbH MPA-3 Multiparameter Data Acquisition System records each particle detection event on the hard disk in list mode data which can be processed off-line later though the same system provides the on-line display of both one- and two-dimensional histograms on the screen and hence easy monitoring of measurements. Both energy and position information are then obtained by performing digital calculations [7]:

$$E = L_1 + E_2 = E_3 + E_4 \tag{1}$$

$$x = L_x\left(\frac{E_3}{E_3+E_4}\right) \tag{2}$$

$$y = L_y\left(\frac{E_1}{E_1+E_2}\right) \tag{3}$$

where L_x and L_y are the x and y lengths of the detector. Additionally, the overall stability and energy resolution of the system was monitored by applying pulser signals to all four preamplifiers.

3. Results

3.1. PSD performance by using a triple alpha-source

Before attempting any practical measurement by using the blocking technique, each PSD was mounted in a small vacuum chamber and a mixed alpha source (^{239}Pu, ^{241}Am, ^{244}Cm) was used in order to optimize the amplifier gains thereby determining its energy resolution at full width half maximum (FWHM). Both the influence of the bias voltage and shaping time constant on the FWHM were also evaluated under the same conditions. The alpha source was kept at a distance of 15 cm with respect to the PSD. Following this procedure, it was found that if a bias of 20 V is applied over the PSDs and a shaping time of $\tau = 2.0\ \mu$s is used, then from the 5.486 MeV ^{241}Am peak in the alpha spectra an energy resolution of 33 keV FWHM is measured for the Silicon Sensor PSD while a better energy resolution of 22 keV FWHM is obtained for the SiTeK PSD. Fig. 3 shows the best alpha spectrum for the Silicon Sensor PSD where, in addition to the intense principal lines, the fine structure weak transitions from the decay of the three nuclides are clearly seen.

In order to determine the position resolution ideally a diaphragm with very small holes should be used, but this would require excessively long counting times, therefore larger diameter holes are better suited. In this way, the same abovementioned setup was used for the determination of the position resolution, but this time a 1 mm thick aluminum mask was interposed between the alpha source and the PSD. This mask was placed at 2.0 mm in front of the detector surface and it contains a square array of 5×5 pinholes, 0.5 mm each in diameter (D) with a 1.8 mm internal distance. Besides, on top of the mask a shield was mounted in order to cover the PSD when not in use. The two-dimensional position pattern obtained for the Silicon Sensor PSD by using 0.5 μs shaping time is shown in Fig. 4. It was considered that measured position patterns will be a convolution of the detector resolution with the position probability distribution defined by the holes ($\sigma_h = \mathrm{D}/\sqrt{12} = 0.144 \pm 0.014$ mm). Assuming

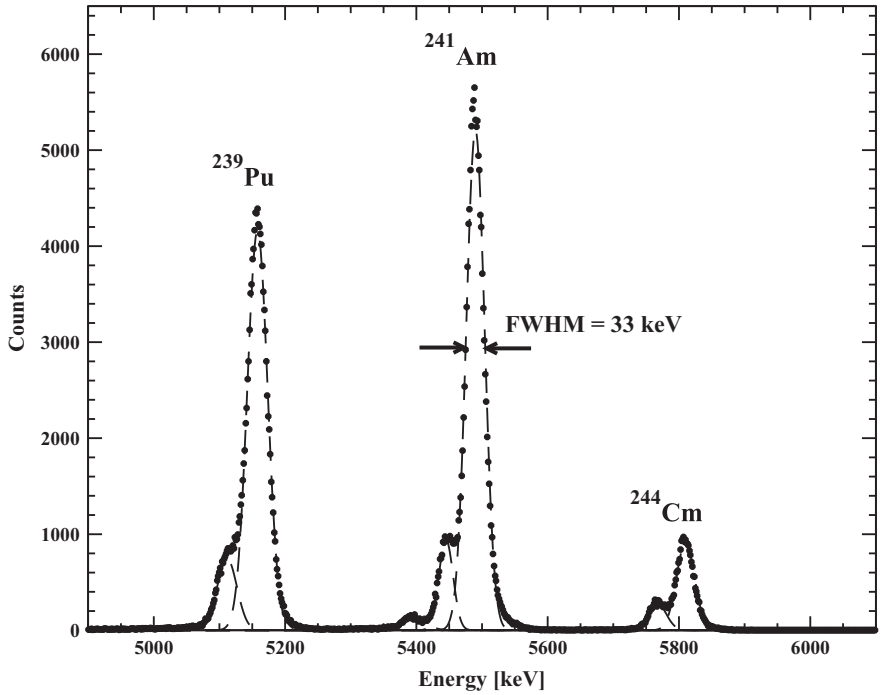

Fig. 3. Energy spectrum from a triple alpha source containing ^{239}Pu, ^{241}Am and ^{244}Cm obtained with a PSD Silicon Sensor. The fitted line shape of the 5.486 MeV ^{241}Am peak gives an energy resolution FWHM = 33 keV if a shaping time $\tau = 2\ \mu$s is used.

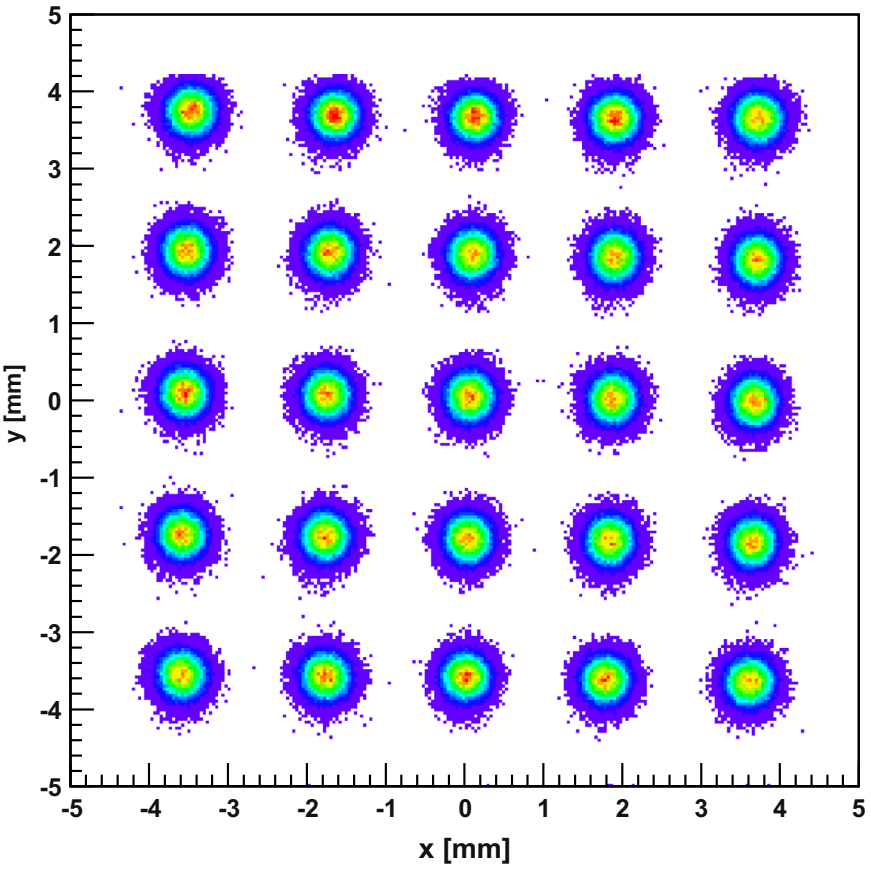

Fig. 4. Two-dimensional position pattern measured with an alpha source and a mask with 5×5 pinholes in front of the PSD surface. As described in the text, a position resolution of the detector 0.072 mm (standard deviation) was obtained if the pulse shaping time constant was 0.5 μs.

that both distributions can be represented by gaussian functions therefore a two-dimensional gaussian fit was applied to each spot of Fig. 4 giving rise to a measured resolution ($\sigma_{exp} = 0.1614 \pm 0.0012$ mm). For the Silicon Sensor PSD the average detector position resolution thus obtained was $\Delta L = \sqrt{\sigma_{exp}^2 - \sigma_h^2} = 0.072 \pm 0.029$ mm (standard deviation) while for the SiTeK PSD this measurement was not carried out since, as will be explained below, this detector began to show significant deterioration in its performance.

Our energy resolution achieved for the SiTek detector is somewhat worse than reported in Ref. [7] although in that work a similar PSD from the same manufacturer was used. However, this may be a consequence of the intrinsic energy resolution of the alpha source used in our tests. Also note that for RCD-PSDs with larger area, such as 20×20 mm^2 in Ref. [9], typically worse values for both energy and position resolution are reached. The fact that energy and position resolution are optimized for different values of the amplifier shaping time constant is explained in the next section.

3.2. PSD performance under ion beam conditions

To measure the characteristics of this position sensitive detector under normal RBS/C conditions, a 2.0 MeV helium ion beam was produced by using a 2.5 MV Van de Graaff accelerator located at the Ion Beam Laboratory of the Instituto Tecnológico e Nuclear (ITN/IST) in Lisbon. The PSD was installed in a RBS/C chamber at an angle of 140° in relation with the beam direction while a surface barrier detector (SSB) located at 165° was additionally used to compare the performance of both sensors. The same process of optimizing the acquisition system mentioned above was performed again but this time using an ion beam current of 5 nA impinging on a thin Au/SiO_2/C multilayer sample with a well-known concentration deposited on a carbon substrate. At the chamber entrance a 0.5 mm collimator was installed, while the distance between the sample and the detector was 100 mm. From Fig. 5, the RBS spectra collected simultaneously by both detectors show that if the shaping time is set to 2.0 μs for the PSD and 0.5 μs for the SSB, then the best energy resolution achieved under ion beam conditions are $\Delta E = 37$ keV and $\Delta E = 13.0$ keV (FWHM) for the PSD and the SSB detectors, respectively.

Subsequently, the shaping time for the PSD was set to 0.5 μs, the steel mask was interposed between the sample and the PSD and also the beam current was increased up to 50 nA in order to give rise to two new two-dimensional patterns. The first one was obtained by setting a ROI around the Au peak while for the second pattern another ROI was set around the silicon signal. By analyzing every spot of these patterns it follows that the position resolution under these conditions were $\Delta L = 0.080 \pm 0.026$ mm (standard deviation) for the gold peak at ~ 1.85 MeV (very similar to the alpha source value) and $\Delta L = 0.247 \pm 0.010$ mm (standard deviation) for the Si peak at ~ 1.1 MeV as can be observed in Fig. 6. However, when the shaping time is set again to 2.0 μs the position resolution for the gold peak worsen to 0.189 ± 0.014 mm. The fact that position and energy resolution are optimized for different amplifier shaping time settings, results from an intricate combination of several effects. On the one hand, the noise in each of the position signals E_1, E_2, E_3, and E_4 is to a large extent dominated by the Johnson noise in the dividing resistors, which is minimized by the use of short shaping time constants [6]. However, the noise in opposite contacts on the same side of the detector is anti-

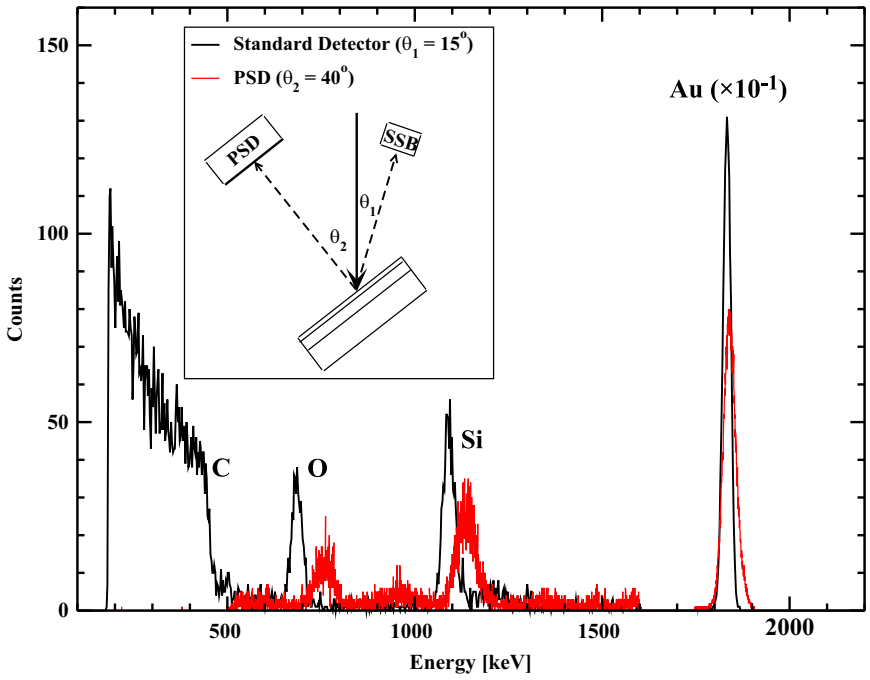

Fig. 5. Energy spectra of backscattered 2.0 MeV ^{4}He ions from an Au/SiO_2/C sample collected simultaneously by both standard (SSB) and PSD detector. The Au peak has been normalized in order to show both spectra more clearly. The inset depicts the position of both detectors and the sample with respect to the incident beam. The measured FWHM of the Au peak was 31 keV with the SSB and 46 keV with the PSD. The natural width of the Au peak is 28 keV, meaning the detector resolution was 13 keV for the SSB and 37 keV for the PSD. Note that the O and Si peaks for the two detectors are shifted as a result of the different measurement geometries.

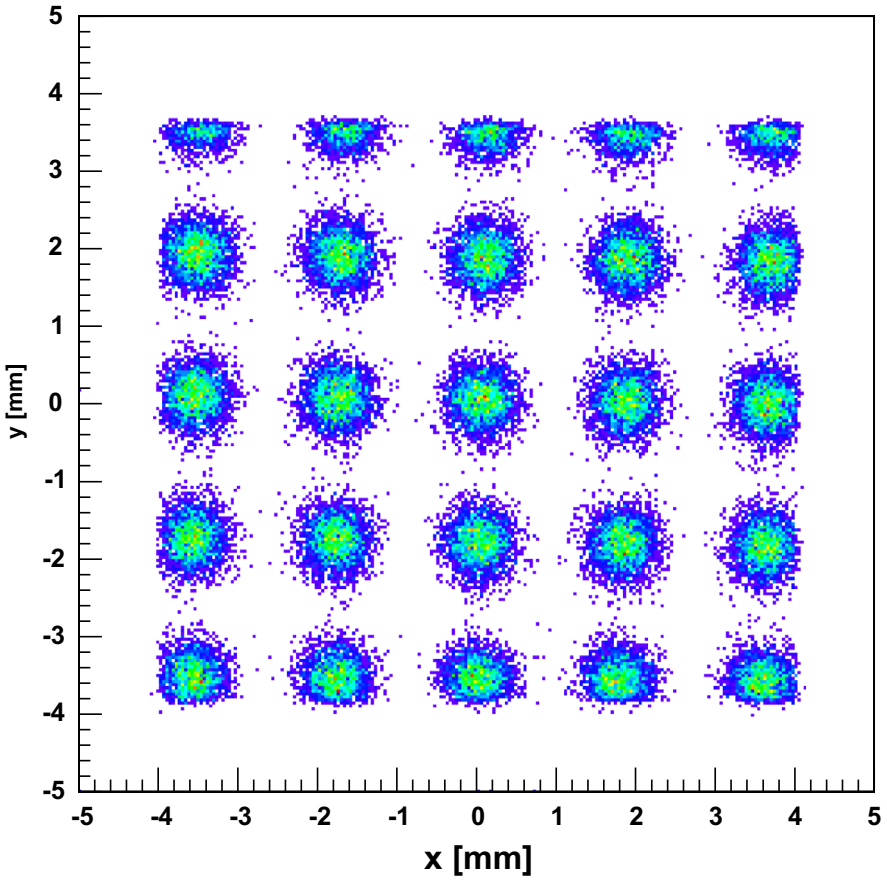

Fig. 6. Two-dimensional position pattern measured with 2.0 MeV ^{4}He ions from an Au/SiO_2/C sample when a ROI is set around the silicon signal and a mask with 5×5 pinholes is in front of the PSD surface.

correlated, so that a large part of this noise is eliminated when adding the two signals to calculate the energy signal. As a result, the noise characteristics of the two energy signals E_1+E_2 and E_3+E_4 are more similar to plain capacitive noise resulting from the detector capacitance and can be minimized by long shaping time constants.

On the other hand, there is the effect of ballistic deficit, which is well known [6,9,18,20] to pose a major limitation for this type of PSD: variations in the time it takes to collect the charges arising from different locations within the detector lead to variations in pulse shape, resulting in non-linear response to pulse height inside the main amplifier. This degrades the integral energy resolution of the detector and also introduces distortions in the position accuracy. Ballistic deficit is e.g. responsible for the fact that a better energy resolution is obtained if one only registers events from the center of the detector, instead of integrating over its whole area. The effect of ballistic deficit is generally minimized by the use of long shaping time constants.

Besides considering energy resolution, position resolution and linearity, the choice of shaping time constant is also influenced by the fact that shorter shaping times lead to less pile-up effects at high count rates, and thus always has to reflect a compromise between different experimental requirements. For instance, a shaping constant $\tau = 0.5$ μs was set in order to carry out studies of lattice location since in this case a better position resolution is required. This experimental setup allows data-taking rates of up to about 1 kHz corresponding to measuring times of about 10–20 min for recording a meaningful two-dimensional spectrum containing typically around 10^6 events. It should be noted that if the beam current is increased even further the spectra start to show distortions due to pile-up effect.

Regarding the possible radiation damage, it is worth noting that after several experiments under ion beam analysis conditions and fluences of the order of 4×10^8 part/cm^2, the Silicon Sensor PSD performance did not show any noticeable deterioration, including the absence of significant changes in the inter-electrode resistance measurements. On the other hand, the SiTek PSD failed after less than 2 days of RBS/C beam time and an alpha particle flux less than 5×10^6 part/cm^2. Since often a radiation tolerance around 10^9 alpha part/cm^2 is quoted for ordinary Si detectors, e.g. in Ref. [21], and since a similar PSD from the same manufacturer used in a previous study [4] had not shown such problems, this behavior was quite unexpected. Closer inspection revealed that the resistance of the front electrode had increased from $\sim$10 kΩ to above 100 kΩ, resulting in loss of position resolution and coincidence between front and back signals. The failure seems hence to be caused by deactivation of the boron (B) acceptors in the front electrode. Similar effects have been reported in previous studies of resistive charge division PSDs [22]

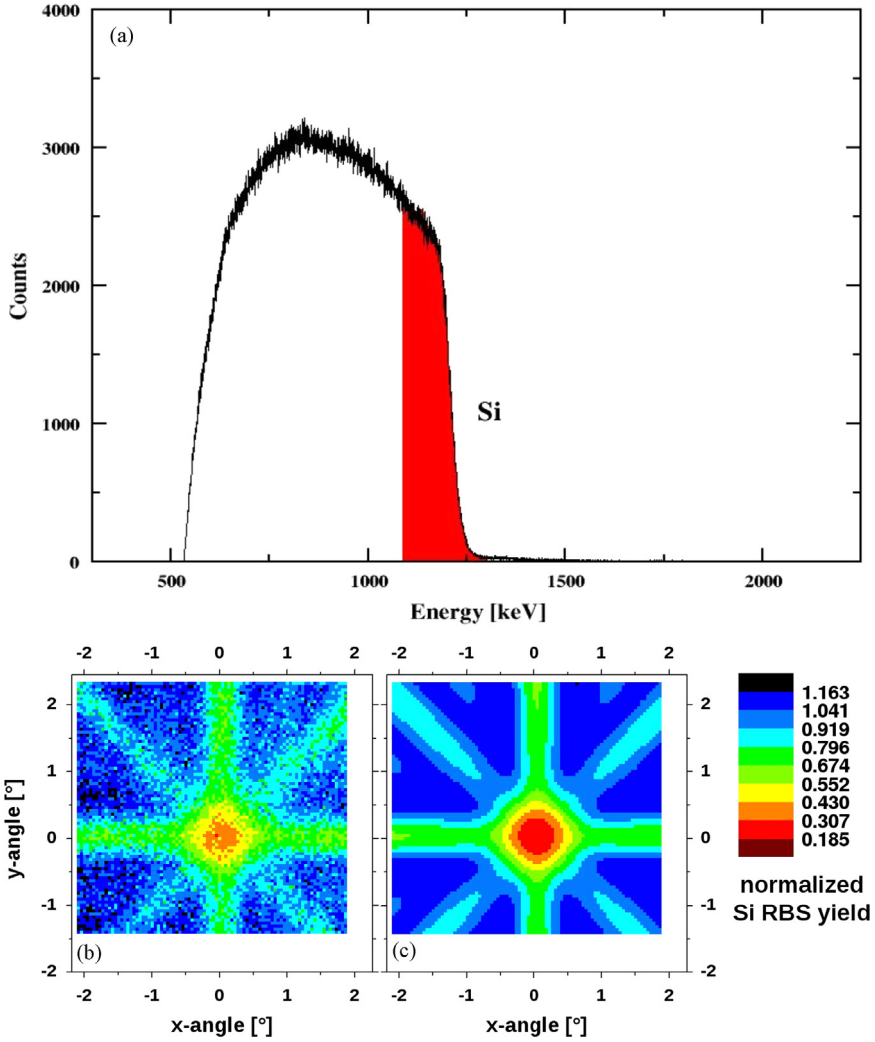

Fig. 7. Measured blocking patterns when 2.0 MeV alpha particles impinge on a Si ⟨100⟩ single crystal sample. (a) RBS spectrum showing in red the ROI set around the silicon edge in order to gate the 2D pattern. (b) Si ⟨100⟩ blocking pattern obtained when the sample is facing the detector while the result for fitting FLUX data to this experimental 2D pattern is shown in (c). (For interpretation of the references to color in this figure caption, the reader is referred to the web version of this paper.)

and were attributed to the buildup of positive charges in the SiO_2 entrance window, which compensate the B acceptors. It hence seems as if the particular design of the entrance window and front electrode of the SiTek 2L10UV_SU72 detector makes it unsuitable for ion beam analysis applications.

3.3. Rutherford backscattering studies in blocking geometry

Several experiments were performed in order to characterize the performance of the Silicon Sensor PSD for RBS/C in blocking geometry with 2.0 MeV alpha particles. In the first experiment a Si ⟨100⟩ single crystal sample was used. In order to obtain a 2D blocking pattern, a region of interest (ROI) around the Si edge was set in the corresponding RBS spectrum depicted in Fig. 7a, corresponding to particles backscattered from Si atoms in a depth window of 0–2000 Å from the surface. The sample was then rotated in order that the ⟨100⟩ surface direction was facing the detector, and data acquired for approximately 2 h at a count rate of 1 kHz with a beam current of 5 nA. The measured 2D pattern in Fig. 7b clearly shows the channeling effects of the axial ⟨100⟩ and the families of planar (110) and (100) directions. The quantitative analysis of the pattern was performed by comparing it to a number of simulated patterns obtained by using the Monte Carlo simulation code FLUX [23]. The fact that FLUX, which simulates the trajectories of channeling ions entering a single crystal, can be applied also to the case where particles originating from emitters inside a crystal are blocked on their way out, exploits the reciprocity theorem of channeling, which is essentially based on the time reversal of ion trajectories in a single crystal. As has been demonstrated in Ref. [4], this approach is feasible as long as the energy loss of the alphas along the trajectory does not become too pronounced. For the present purpose FLUX simulations were run for a starting energy of 1204 keV, which corresponds to the energy of alpha particles backscattered from Si atoms at the surface of the sample. As value for the rms displacement of Si atoms at room temperature $u_1=0.0825$ Å was used, derived from a Debye temperature of $T_D=490$ K, which is well established for FLUX simulations of that material [24]. A number of α emission patterns were then simulated for the angular range of $\pm 3^\circ$ with a step width of 0.05°, varying the angular resolution standard deviations in between 0.04° and 0.4°. The experimental result in Fig. 7b was then successively fitted by theoretical patterns for different angular resolutions σ, using fitting procedures outlined in Ref. [4]. The best fit was obtained for $\sigma=0.21^\circ$ and the fitted pattern is shown

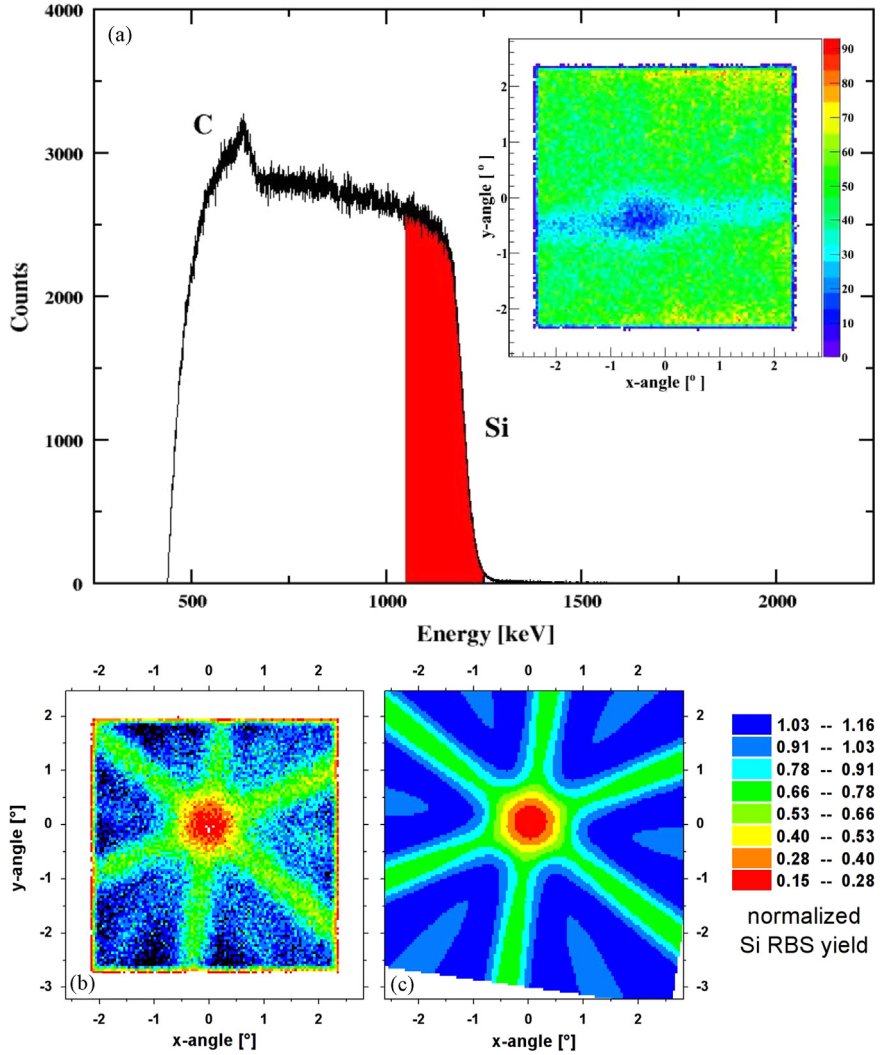

Fig. 8. Measured blocking patterns when 2.0 MeV alpha particles impinge on a 6H-SiC virgin sample. (a) RBS spectrum showing in red the ROI set around the silicon edge in order to gate 2D pattern. (b) 6H-SiC ⟨0001⟩ blocking pattern obtained when the sample is facing the detector while the result for fitting FLUX data to this experimental 2D pattern is shown in (c). Additionally, the inset of (a) shows the 6H-SiC ⟨$\bar{1}$101⟩ blocking pattern obtained when the sample is rotated 17° respect to the above angular position. (For interpretation of the references to color in this figure caption, the reader is referred to the web version of this paper.)

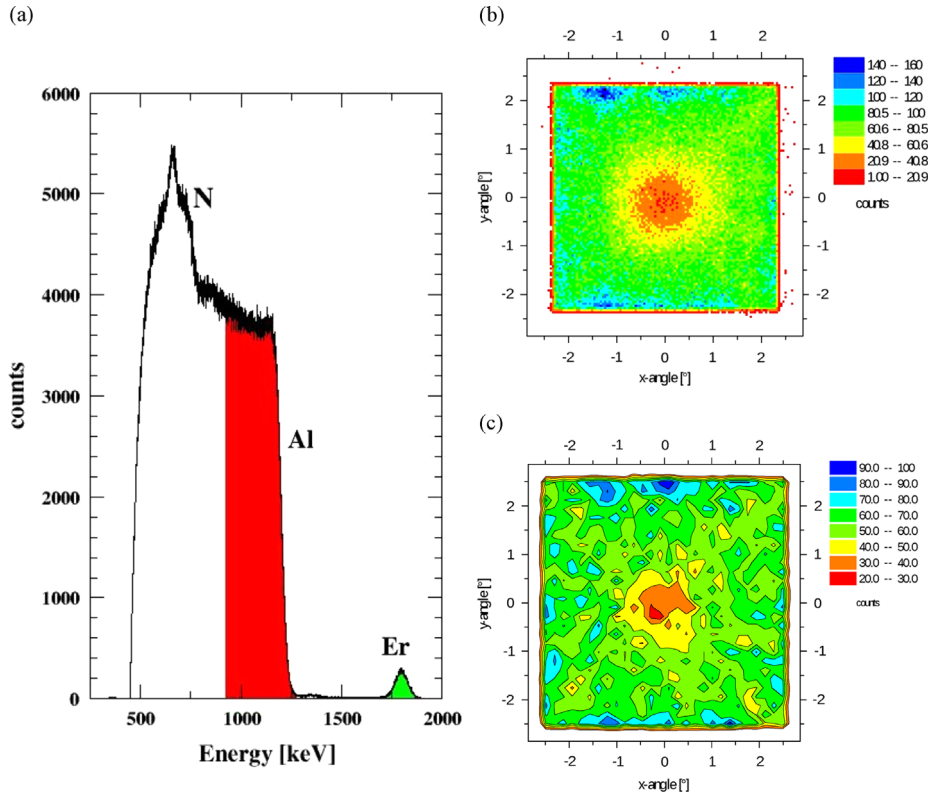

Fig. 9. Measured blocking patterns when 2.0 MeV alpha particles impinge on a AlN:Er (1×10^{15} at/cm^2) implanted sample. (a) RBS spectrum acquired when the sample is facing the detector $\theta_2 = 40^\circ$. (b) AlN ⟨0001⟩ blocking pattern of alphas backscattered from aluminium (red ROI in RBS spectrum) (c) AlN:Er ⟨0001⟩ blocking pattern of alphas backscattered from Er implanted into AlN film (green ROI in RBS spectrum). (For interpretation of the references to color in this figure caption, the reader is referred to the web version of this paper.)

in Fig. 7c . According to the fit results, the measured pattern exhibited a minimum yield of $\chi_{min}=0.185$ with an isotropic background of 5.7%. The isotropic background can be a result of damage in the sample. When its value was fixed at 0% during the fit, the best fit was obtained for $\sigma=0.22^\circ$, corresponding to $\chi_{min}=0.153$, hence quite similar values. The angular resolution of $\sigma=0.21^\circ$ indicated by the best fit result can be compared to what is estimated from the size of the beam spot and the position resolution of the detector, taking into account the geometry of the setup. For that purpose the beam spot size of 0.5 mm diameter is approximated by a Gaussian distribution of 0.145 mm with the same standard deviation. Using the position resolution standard deviation of 0.25 mm for ^{4}He particles backscattered from Si and the distance of 100 mm from detector to sample, one estimates an angular resolution of 0.17°, in reasonable agreement with the best fit results of FLUX simulations.

The setup was then used to measure the blocking patterns of 2 MeV ^{4}He particles from a 6H-SiC ⟨0001⟩ single crystal (commercial sample obtained from CrysTec GmbH). The corresponding energy spectrum is shown in Fig. 8a. Similar as in the case of the Si sample, a ROI was set for ^{4}He particles backscattered from Si atoms in the depth range of 0–2000 Å. The resulting angular emission pattern in Fig. 8b shows the axial ⟨0001⟩ blocking effect, as well as the family of major $(11\bar{2}0)$ planes. Performing FLUX simulations in this case, however, proved a bit more of a challenge, owing to the fact that the Debye temperatures reported for SiC in the literature vary considerably, e.g. 777 K [25], 851 K [26], 961 K [27], 1195 K [28], 1200–1300 K [29], 1472 K [30]. If one uses e.g. the rms displacements of Si and C atoms corresponding to $T_D=1200$ K, i.e. $u_1(Si)=0.0440$ Å and $u_1(C)=0.0492$ Å, as input in FLUX, then the best fit to the experimental results is obtained for an angular resolution of 0.23° and indicates an amorphous fraction of 14.2% with a minimum yield of 0.207. On the other hand, if $u_1(Si)=0.0603$ Å and $u_1(C)=0.0611$ Å [26] is used, corresponding to $T_D=851$ K, the best fit is obtained for an angular resolution of 0.24°, indicating an amorphous fraction of 1.6% only, with a minimum yield of 0.154. These latter results would confirm a good quality of the SiC sample and are shown in Fig. 8c. Summarizing, despite of the uncertainty in the correct values for the rms displacement of the Si and C atoms, the angular resolution in both cases was in good agreement with the value obtained from the Si sample. Following the ⟨0001⟩ measurement, the sample was rotated to the ⟨1101⟩ axis, whose blocking pattern is shown as inset in Fig. 8a.

In another experiment the Silicon Sensor PSD was used to carry out lattice location study of Er ions implanted into AlN. The sample, an AlN film with thickness of 3 μm grown by hydride vapour phase epitaxy (HVPE) on a sapphire substrate, was purchased from TDI, and implanted with 150 keV Er+ ions with a fluence of 1×10^{15} at/cm^2 at a 10° tilt angle between the ion beam and the surface normal. Fig. 9a presents the corresponding RBS spectrum of 2 MeV alphas where the Er implantation peak is clearly observed. A ROI around the Al edge (in red) and the Er peak (in green) were set in order to extract the 2-dimensional [0001] blocking patterns from the Al host atoms (Fig. 9b) and the Er impurities (Fig. 9c). With a beam current of 4 nA, count rate 1 kHz and an irradiation time of about 3.5 h the measured minimum yields were $\chi_{min}(Al)=23\%$ and $\chi_{min}(Er)=50\%$, respectively. The results show that about 2/3 of Er is incorporated along the AlN *c*-axis, most likely on substitutional Al-sites. The Silicon Sensor PSD therefore seems suitable to carry out lattice location studies for an areal concentration of $\sim 1 \times 10^{15}$ at/cm^2 of heavy impurities, e.g. in Si, SiC or AlN single crystals.

4. Conclusion

Although resistive charge division position-sensitive photodiodes were designed for optical applications, the RBS/C measurements and tests performed in this work confirm that they can be also useful tools in ion beam analysis (IBA). However, not all detector types are able to withstand the radiation damage under typical IBA conditions, so that this needs to be tested for specific models from a manufacturer. Due to its principle of operation and the related noise characteristics and non-linearities, the integral energy resolution of a RCD-PSD is not as good as ordinary Si detectors, but also not much worse than e.g. an annular Si detector. The angular resolution achieved with a suitable $10 \times 10\ mm^2$ RCD-PSD using a 0.5 mm collimated 2 MeV He beam backscattered from Si, SiC or AlN samples, is around 0.21°. This allows performing lattice location studies of 1×10^{15} at/cm^2 of heavy impurities by means of the blocking effect, although in this energy range the angular resolution is worse than when using the RBS/C technique with conventional, non-position sensitive detectors. However, since the performance of RCD-PSDs considerably improves at higher particle energies, they should be excellent tools e.g. for performing RBS/C studies at beam energies around 4–5 MeV, as they are for instance available with Tandem accelerators. A particular advantage of the use of a PSD e.g. in RBS/C studies is the relatively simple process of orienting the sample with respect to the detector.

Acknowledgments

The authors gratefully acknowledge the invaluable contribution of M. Cabaça and F. Baptista from ITN/IST for their constant availability and the great quality when tooling the detector vacuum housing. K. Lorenz is acknowledged for providing the AlN:Er sample. The authors recognize financial support from the Portuguese Foundation for Science and Technology through CERN/FP/123585/2011 and PTDC/CTM/100756/2008 as well as the SPIRIT project, EC Grant Agreement no. 227012-CP-CSA-Intra.

References

[1] H. Nolte, W. Assmann, H. Huber, S.A. Karamian, H.D. Mieskes, Nuclear Instruments and Methods in Physics Research Section B 136 (1998) 587.
[2] D.S. Gemmell, Reviews of Modern Physics 46 (1974) 129.
[3] H. Hofsäss, G. Lindner, Physics Reports 201 (1991) 123.
[4] U. Wahl, Physics Reports 280 (1997) 145.
[5] K.H. Lauterjung, J. Pokar, B. Schimmer, R. Studner, Nuclear Instruments and Methods in Physics Research 162 (1963) 117.
[6] E. Lægsgaard, Nuclear Instruments and Methods in Physics Research 162 (1979) 93.
[7] M. Lindroos, Ö. Skeppstedt, Nuclear Instruments and Methods in Physics Research Section A 306 (1991) 225.
[8] D.P.L. Simons, P.H.A. Mutsaers, L.J. van IJzendoorn, M.J.A. de Voigt, Nuclear Instruments and Methods in Physics Research Section B 139 (1998) 273.
[9] K. Kovačević, M. Zadro, Nuclear Instruments and Methods in Physics Research Section A 423 (1999) 103.
[10] J. Räisänen, O. Harju, G. Tjurin, I. Riihimäki, Review of Scientific Instruments 72 (2001) 4358.
[11] E. David-Bosne, Timepix and FitPix detection system for RBS/C material analysis (M.Sc. thesis) Universidade de Aveiro, Portugal, 2013. ⟨http://cds.cern.ch/record/1640586/files/CERN-THESIS-2013-239.pdf⟩.
[12] J. Jakubek, Nuclear Instruments and Methods in Physics Research Section A 576 (2007) 223.
[13] J. Jakubek, A. Cejnarova, T. Holy, S. Pospisil, J. Uher, Z. Vykydal, Nuclear Instruments and Methods in Physics Research Section A 591 (2008) 155.
[14] W.K. Chu, J.W. Mayer, M.A. Nicolet (Eds.), Backscattering Spectrometry, Academic Press, New York, 1978.
[15] M.L. Swanson, Reports on Progress in Physics 45 (1982) 47.
[16] L.C. Feldman, J.W. mayer, S.T. Picraux, Materials Analysis by Ion Channeling, Academic Press, New York, 1982.
[17] J.R. Tesmer, M. Nastasi, J.C. Barbour, C.J. Maggiore, J.W. Mayer, Handbook of Modern Ion Beam Materials Analysis, Materials Research Society, Pittsburg, 1995.
[18] T. Yanagimachi, T. Doke, N. Hasebe, T. Imai, T. Kashiwagi, J. Kikuchi, T. Kohno, W.P. Liu, K. Munakata, T. Motobayashi, H. Murakami, K. Nagata, A. Nakamoto, H. Yamaguchi, Nuclear Instruments and Methods in Physics Research Section A 275 (1989) 307.
[19] A. Banu, Y. Li, M. McCleskey, M. Bullough, S. Walsh, C.A. Gagliardi, L. Trache, R.E. Tribble, C. Wilburn, Nuclear Instruments and Methods in Physics Research Section A 593 (2008) 399.
[20] G.F. Knoll, Radiation Detection and Measurement, 2nd ed., John Wiley & Sons, New York, 1989.
[21] W. De Coster, B. Brijs, W. Vandervorst, P. Burger, Nuclear Instruments and Methods in Physics Research Section B 64 (1992) 287.
[22] K. Teraoka, M. Nakamura, H. Tajima, K. Niwa, H. Tanaka, K. Yamamura, K. Yamamoto, K. Kodama, Nuclear Instruments and Methods in Physics Research Section A 324 (1993) 276.
[23] P.J.M. Smulders, D.O. Boerma, Nuclear Instruments and Methods in Physics Research Section B 29 (1987) 471.
[24] A. Dygo, P.J.M. Smulders, D.O. Boerma, Nuclear Instruments and Methods in Physics Research Section B 64 (1992) 701.
[25] J. Schardt, J. Bernhardt, U. Starke, K. Heinz, Surface Review and Letters 5 (1998) 181.
[26] H. Schulz, K.H. Thiemann, Solid State Communications 32 (1979) 783.
[27] Y.F. Hu, F.J. Kong, C. Zhou, Acta Physico-Chimica Sinica 24 (2008) 1845.
[28] T.H. Peng, Y.F. Lou, S.F. Jin, W.Y. Wang, W.J. Wang, G. Wang, X.L. Chen, Powder Diffraction 24 (2009) 311.
[29] Y. Goldberg, M.E. Levinshtein, S.L. Rumyantsev, in: M.E. Levinshtein, S.L. Rumyantsev, M.S. Shur (Eds.), Properties of Advanced Semiconductor Materials GaN, AlN, SiC, BN, SiC, SiGe, John Wiley & Sons, Inc., New York, 2001, p. 93.
[30] S. Stelmakh, E. Grzanka, M. Wojdyr, T. Proffen, S.C. Vogel, T.W. Zerda, W. Palosz, B. Palosz, Zeitschrift für Kristallographie 222 (2007) 174.